Miner Deposita (2006) 41: 323–338
DOI 10.1007/s00126-006-0049-7

ARTICLE

Francesca Castorina · Umberto Masi · Giorgio Padalino · Marcella Palomba

Constraints from geochemistry and Sr–Nd isotopes for the origin of albitite deposits from Central Sardinia (Italy)

Received: 12 July 2005 / Accepted: 29 December 2005 / Published online: 19 May 2006

Abstract Major- and trace-element contents and Sr–Nd isotope ratios were determined in albitite, albitized and unaltered late-Variscan granitoid samples from the world-class Na-feldspar deposits of central Sardinia, Italy. The albite deposit of high economic grade has geological, textural, and chemical features typical of metasomatic alteration affecting the host granitoids. Albitization, locally accompanied by chloritization and epidotization, was characterized by strong leaching of Mg, Fe, K, and geochemically similar trace elements, and by a significant increase of Na. Ca, and P were moderately leached in the most metasomatized rocks. Other major (Si, Ti, Ca) and trace elements (U, Th, Y, and Zr), along with light (LREE) and middle (MREE) rare-earth elements, behaved essentially immobile at the deposit scale. The Nd-isotope ratios (0.512098 to 0.512248) do not provide information on the emplacement age of the unaltered late-Variscan granitoids. On the other hand, their Sr-isotope ratios fit an errorchron of 274±29 Ma (1σ error), in fair agreement with all published ages of Sardinian Variscan granitoids. The very low Rb content of albitized rocks precludes application of the Rb–Sr radiometric system to determine the age of albitization. The Sm–Nd system is not applicable either, because the $^{143}Nd/^{144}Nd$ ratios of albitized rocks and unaltered granitoids overlap. The overlap confirms that Sm and Nd were substantially immobile during albitization. On the other hand, the measured $^{87}Sr/^{86}Sr$ ratios of the albitized rocks are appreciably lower than those of the unaltered host granitoids, whereas, their initial Sr-isotope ratios are higher. This seems to suggest that a) albitization was induced by non-magmatic fluids rich in radiogenic Sr, and b) albitization occurred shortly after the granitoid emplacement. This conclusion is supported by Nd isotopes, because unaltered granitoids and albitites fit the same reference isochron at 274 Ma. The fluids acquired radiogenic Sr by circulation through the Lower Paleozoic metasedimentary basement. Specifically, it is estimated that Sr supplied by the non-carbonatic basement represents about 22 wt% of total Sr in albitite.

Keywords Albitite · Geochemistry · Sr–Nd isotope ratios · Metasomatism · Sardinia

Editorial handling: R. Moritz

F. Castorina · U. Masi
Dipartimento di Scienze della Terra,
Università La Sapienza di Roma,
Piazzale Aldo Moro 5,
00185 Rome, Italy

F. Castorina · U. Masi
IGAG-CNR, Istituto di Geologia Ambientale e Geoingegneria,
Consiglio Nazionale delle Ricerche, Sezione di Roma,
c/o Università La Sapienza di Roma,
Piazzale Aldo Moro 5,
00185 Rome, Italy

G. Padalino
Dipartimento di Geoingegneria e Tecnologie Ambientali,
Università di Cagliari,
Piazza d'Armi 19,
09123 Cagliari, Italy

M. Palomba (✉)
IGAG-CNR, Istituto di Geologia Ambientale e Geoingegneria,
Consiglio Nazionale delle Ricerche, Sezione di Cagliari,
c/o Università di Cagliari,
Piazza d'Armi 19,
09123 Cagliari, Italy
e-mail: mpalomba@unica.it
Tel.: +39-070-6755540
Fax: +39-070-6755511

Introduction

The geochemical features of albitization of granitoids have been widely documented (e.g., Carten 1986; Leroy and Turpin 1988; Turpin et al. 1988; Charoy and Pollard 1989; Dilles and Einaudi 1992; Dilles et al. 1995; Abdalla et al. 1996). The origin of the most common albitite types is ascribed to the action of metasomatic-hydrothermal fluids on granitoids (e.g. Kovalenko 1978; Cheilletz and Giuliani 1982; Chauris 1985; Cathelineau 1988). This type of albitite

usually forms along fractures in host granitoids, and is characterized by quartz leaching from the protolith and deposition of new minerals. Commonly, it shows overlapping features of hydrothermal and supergene stages (Leroy and Turpin 1988), and is accompanied by a distinctive alteration facies ("episyenite") and/or by U mineralization (e.g., Cathelineau 1987; Schoch and Scheepers 1990; Turpin et al. 1991; Bachiller et al. 1997, Petersson and Eliasson 1997). A subordinate type of albitite is represented by direct crystallization from Na-rich magmas. It is recognizable by a typical *snowball quartz* texture (Schwartz 1992).

In this paper, we describe the albitite occurrences spread over an area of about 90 km^2 around the villages of Orani and Ottana in central Sardinia. Collectively, these deposits represent the most important feldspar resource in Europe and in the world, both for side and production. The central Sardinian deposits produce about 600,000 t per year (t/y), compared to an Italian and world feldspar production of the order of 2.5 and 10 million t/y, respectively (Potter 2004). The Sardinian albitite is sold in Italy and Spain, mainly for the production of technical and glazed porcelain stoneware. It is also used in glass production as a contributor of Al_2O_3 and Na_2O. A chlorite-bearing variety of Sardinian albitite is a powerful flux, which allows sinterization at temperatures lower than other traditional feldspathic material.

The Sardinian albitites are hosted by late-Variscan granitoids. They are devoid of sulfides, carbonates, and fluorides and are not accompanied by either episyenitization or U mineralization. The origin of these rocks was long debated until the 1990s, when a general agreement was achieved on their formation through the action of metasomatic Na- and Mg-rich fluids, which affected the granitoids during the late stage of Variscan orogeny (Bornioli et al. 1993, 1996, 1997). However, these studies ascertained neither the source of the metasomatic fluids, nor the age of albitization. This study provides new geochemical and mineral chemistry data of both albitites and parent rocks, giving additional information on the nature of the metasomatizing process and on physical–chemical characteristics of fluids. In addition, studies on Sm–Nd and Rb–Sr isotopic systems provide constraints on the age of mineralization and on the possible fluid sources.

Geological setting and general features of the mineralization

In this paper, we studied mainly samples from the largest albitite open pit in the area, which is located at Punta Is Paduleddas, NW of the village of Orani, on the southern margin of the Tirso River valley (Fig. 1). In addition, samples from the albitite open pit south of Ottana and from a number of unexploited occurrences, found mainly southwest of Punta Is Paduleddas, were also studied.

The oldest rocks known in the area are of Ordovician–Silurian age. They are only exposed in the northeastern part of the area (Fig. 1), at Punta Is Paduleddas, and consist of metasandstones, metasiltstones, and subordinate marbles (Elter et al. 1986). These rocks were intruded by granitoid magmas between 310 and 270 Ma during the Variscan orogeny (Del Moro et al. 1975; Bralia et al. 1982; Castorina and Petrini 1989; Tommasini et al. 1995). The synkinematic metamorphism ranges from very low- to low-grade (chlorite zone), with estimated temperatures and pressures ranging from 300 to 360°C and 3–4 kbars, respectively (Carosi et al. 1992).

The study area was also intensively tectonized in the late phase of the Variscan orogeny, with formation of major NE–SW, NW–SE, and E–W trending fault systems. The NE- and E-strike slip faults were re-activated in the Cenozoic, when the rift of the present-day Tirso River valley formed. Lastly, large amounts of calc-alkaline ignimbrite and tuff were outpoured into the Tirso River valley at about 21.5 Ma (Assorgia et al. 1998). This magmatic episode belongs to the Tertiary calc-alkaline volcanic cycle of Sardinia, a major geological event both at a regional scale and in the study area. Several metalliferous and industrial mineral deposits occur in Sardinia as products of important hydrothermal phenomena associated to this volcanic cycle (Fadda 1994; Maccioni et al. 1995; Simeone and Simmons 1999; Simeone et al. 2003).

The albitite bodies are entirely hosted by the late-Variscan granitoids (Fig. 1). The albitite forms vein- or lens-shaped bodies, mainly localized along joints in the granitoids (Fig. 2). It generally constitutes elongated ridges along a NE structural trend, approximately parallel to both the main fault systems of the Tirso River valley (Arthaud and Matte 1975). The albitite exhibits well-developed fractures orthogonal to the late-Variscan fault system.

The transition from unaltered granitoid to albitite is generally gradual over a few meters, locally through an altered granitoid lithotype, which preserves magmatic textures. This transitional rock, henceforth called albitized granitoid, is macroscopically characterized, with respect to unaltered granitoid, by its lighter color, major alteration or lack of potassium feldspar, transformation of biotite into chlorite, and the presence of quartz veinlets. Granitoid alteration is more intense near faults, especially along fault intersections; the intensity of alteration decreases with distance from faults. Field relationships support the hypothesis that albitization was a metasomatic process (Bornioli et al. 1993, 1996, 1997).

The macroscopic characteristics of albitite are variable. It is generally recognizable by its whitish color, but it becomes greenish-yellow where it contains significant amounts of either chlorite or epidote. These two minerals never occur together. In fact, chlorite-bearing albitite mainly occurs near the metasedimentary basement or within the biotite-rich granitoid, where it overprints or partially replaces biotite. In contrast, epidote-rich albitite occurs within the albitite bodies far from the basement, and is closely related to the most intensely metasomatized and fractured zones. The antago-

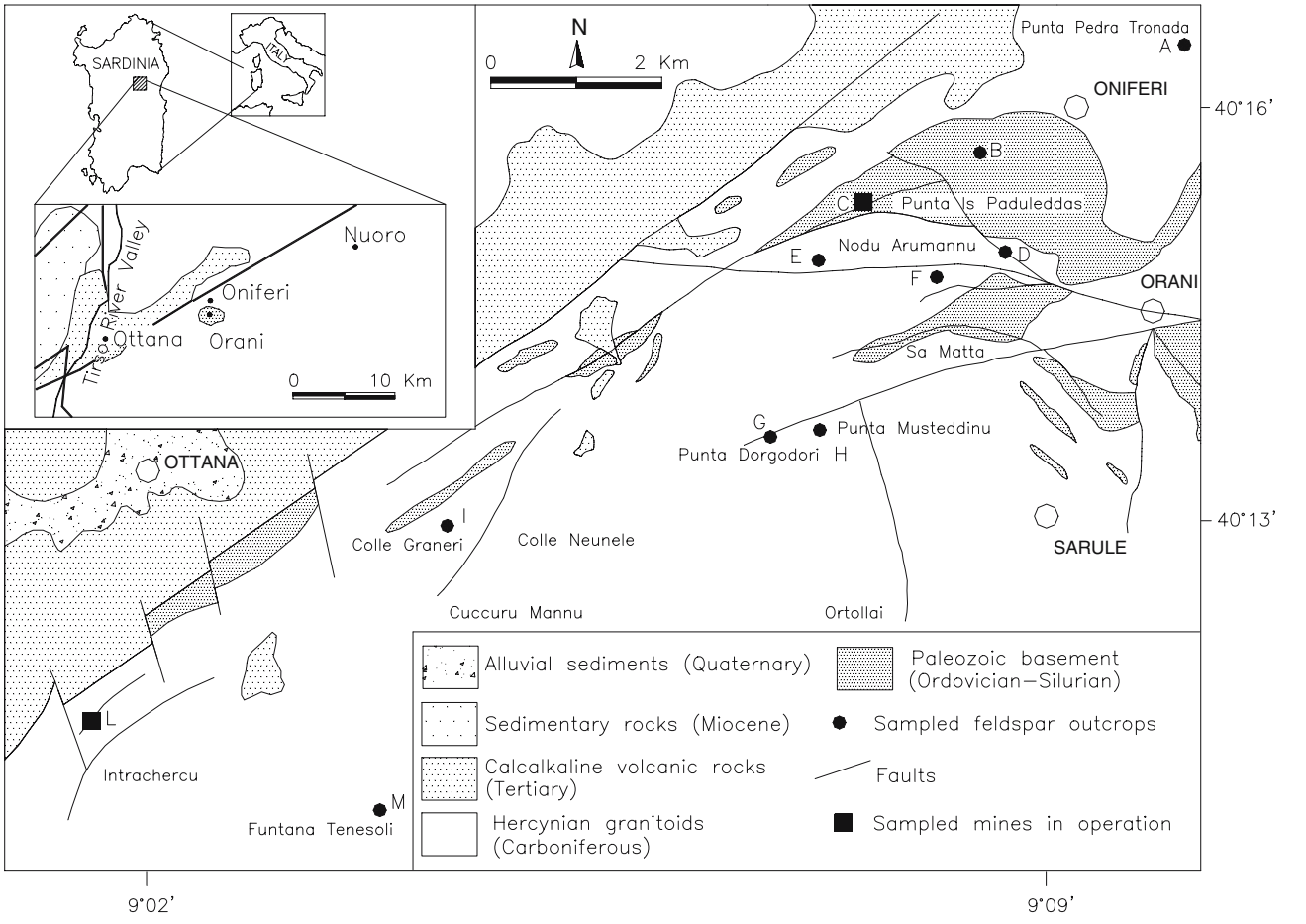

Fig. 1 Geological sketch map of central Sardinia (modified after Bornioli et al. 1993), with locations of the studied samples. The upper inset map shows the location of the investigated area. Lower inset map: basic geology of head of Tirso River valley. The studied samples come from *A* Alb56, *B* Alb27 and Alb28, *C* Alb15 and Alb16, *D* Alb1b, *E* Alb30, Alb31, and Alb34, *F* Alb21, *G* Alb64 and Alb66, *H* Alb40 and Alb44, *I* Alb84, *L* Abo8, Abo11, Abo15, Abo18, Abo19, Abo24, and Abo31, and *M* Alb79 and Alb80

nism between chlorite and epidote may reflect either a different chemistry or a different temperature of formation (higher in the chlorite-rich areas; Bird and Norton 1981).

The igneous textures of the protolith are not preserved in albitite. On a scale of tens to hundreds of meters, depending on the extent of the metasomatic body, albitite occurs in the

Fig. 2 View of a sector of the albitite mine of Punta Is Paduleddas, showing a lens-shaped albitite body (*lighter color*) within granitoid

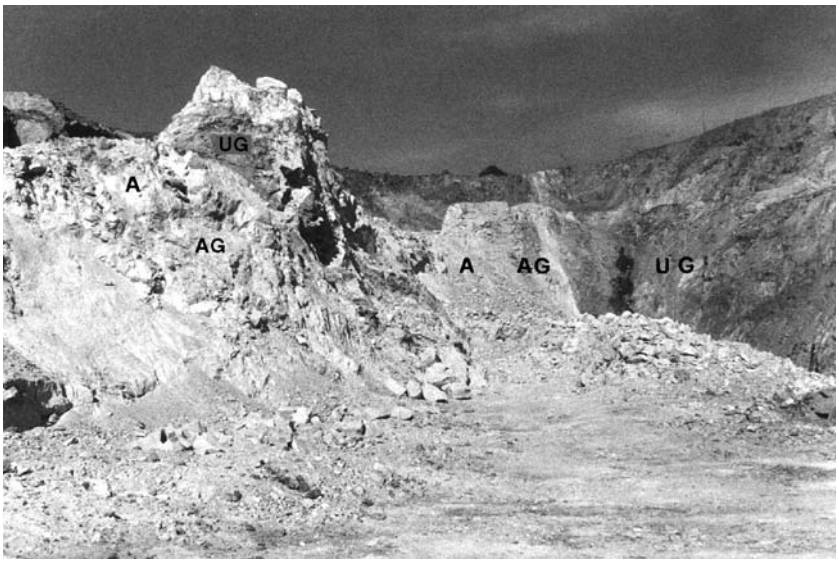

Fig. 3 Typical *patchy zoning* showing albitized (*AG*) and unaltered granitoid (*UG*) cores within albitite body (*A*)

cores of alteration areas, in gradual transition to albitized and unaltered granitoids. On a scale of a few meters, the transition to albitized granitoid is less evident, because the porosity and fracturation of rocks vary considerably, controlling the circulation of metasomatizing fluids and, thus, the intensity of alteration. The *patchy zoning* texture observed in the field, showing either cores of albitized or unaltered granitoid relics within the albitite body (Fig. 3) or the reverse pattern (Fig. 4), probably reflects the variable permeability of the protolith. Evidence of minor dissolution and recrystallization of quartz, occurring in at least three generations, can be recognized at the albitite/unaltered granitoid contact, as well as in the quartz-bearing albitite (Padalino and Palomba 1999). The latter lithotype shows vugs and fractures filled by automorphic quartz, which hosts relics of magmatic quartz. Table 1 summarizes the petrographical features of granitoid, albitized granitoid, and albitite, widely described in previous works (Bornioli et al. 1997; Carcangiu et al. 1996, 1997; Padalino and Palomba 1999; Palomba 2001).

Materials and methods

Feldspars, the most important accessory minerals in albitite, were characterized for chemical composition by means of electron microprobe. REE-bearing mineral phases in albitite were studied by integrated scanning electron microscopy

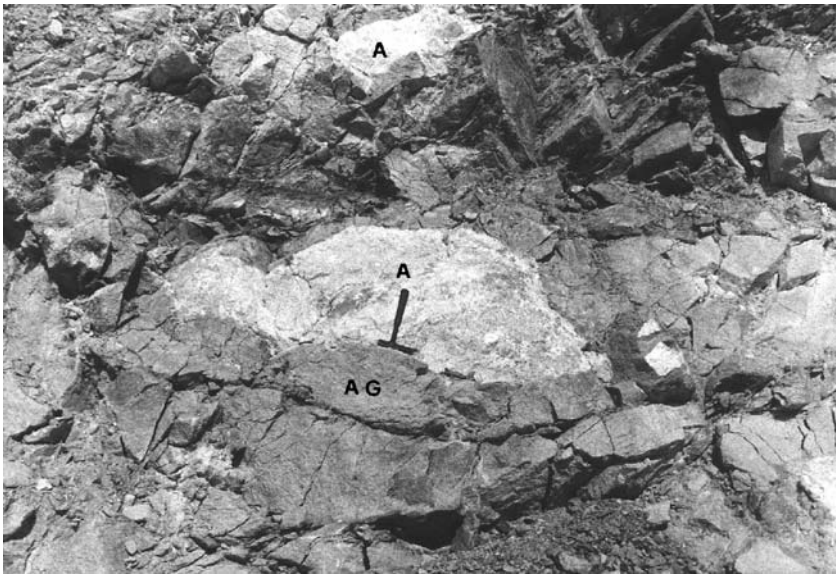

Fig. 4 Typical *patchy zoning* showing albitite cores (*A*) within albitized granitoid (*AG*)

Table 1 Textural and petrographical features of granitoids, albitized granitoids and albitites of central Sardinia

Facies	Textural features	Primary mineral assemblage		Alteration mineral assemblage		Retrograde alteration mineral assemblage
		Main	Accessory	Major	Minor	
Granitoid (from monzogranite to granodiorite)	Equigranular, medium-grained	Plagioclases (granodiorite: An_{40}–An_{45}; monzogranite: An_{20}–An_{25})+ quartz± K-feldspar± biotite	Allanite±apatite± amphibole±zircon± titanite±magnetite± epidote			
Albitized granitoid	Magmatic textures preserved	Quartz+ oligoclase	Allanite±zircon± titanite±magnetite± K-feldspar	Oligoclase+ albite± chloritized biotite	±Quartz (2nd generation)	
Albitite	Magmatic textures never preserved	Albite± quartz	±Oligoclase±zircon± allanite±titanite± K-feldspar	Albite+quartz (up to three generations)± chlorite	±K-feldspar± allanite± epidote± LREE-rich epidote±titanite± oligoclase	±Muscovite± kaolinite± smectites

(SEM) observations and electron probe micro-analyses (EPMA). An A.R.L. microprobe was used in the following conditions: accelerating voltage 20 kV, beam current 20 nA on brass and K_α emission lines. Absolute abundances for REE were determined by comparison with REE-doped synthetic glass standards. Raw data were corrected by the ZAF procedure using the Magic IV program.

The major element composition of unaltered and albitized granitoid and albitite samples was determined by XRF analysis, using a Philips PW 1400 spectrometer equipped with a Rh tube, operating at 30 kV and 60 mA. The "α factors" method was applied to correct matrix effects using a NRLXRF program on standard samples. Loss of ignition (LOI) was determined by heating samples at 900°C for 2 h. With the exception of REE, trace elements were determined by XRF using a Rh tube at 60 kV and 40 mA, and a W tube at 50 kV and 50 mA; data reduction was carried out using a modified version of the NRLXRF fundamental parameter program. Analytical uncertainty for major and trace elements is better than 3 and 5%, respectively.

REE in whole samples were determined by ICP-MS, using a Perkin Elmer Sciex (Elan 5000) instrument, with Rh and Re as internal standards. Sample decomposition was carried out by mixed acid attack (0.2 g sample, 3 ml HF, 3 ml aqua regia, 1 ml $HClO_4$), operating in a microwave oven (Fadda et al. 1995). For accuracy tests, standard reference materials (SRMs) (GSD from 1 to 8, distributed by the Institute of Geophysical and Geochemical Exploration, Langfang, Hebei, China) were used; accuracy values range from ±2 to 5%; precision ranges from ±1 to 2.5% RSD (relative standard deviation); the sensitivity of the method, expressed by MDLs (method detection limits, Fadda et al. 1995), ranges from 0.0032 to 0.050 μg L^{-1}.

Isotopic analyses were performed on selected samples representative of the three groups of rocks studied. Samples for isotopic analyses were decomposed with a mixture of ultrapure HF and HNO_3 in Teflon bombs at 70°C for 48 h, then evaporated to dryness and converted into chloride form using ultrapure 6 N HCl. The same procedure was repeated at 200°C to total dissolution of samples. Some samples were divided into three aliquots, one to determine Sr and Nd isotopic compositions, and the other two, spiked with mixed ^{87}Rb–^{84}Sr and ^{149}Sm–^{150}Nd, to determine elemental concentrations via ID-TIMS. Sr was separated in a 3-ml AG 50 W-X8 resin column. Sm and Nd were separated from the other REE in 2-ml columns filled with hydrogen di-ethylhexylphosphate (HDEHP)-coated Teflon powder, following White and Patchett's (1984) procedure. Isotopic analyses were carried out using a Finnigan MAT 262RPQ multicollector mass spectrometer in static mode. Sr and Nd were run on Re double filaments. The internal precision (within-run precision) of a single analytical result is given as two standard errors of the mean. Repeated analyses of standards gave averages and errors expressed as two standard deviations (2σ), as follows: NBS 987 $^{87}Sr/^{86}Sr = 0.710237 \pm 10$, $^{86}Sr/^{88}Sr$ normalized to 0.1194; La Jolla $^{143}Nd/^{144}Nd = 0.511860 \pm 10$, and

Table 2 Mineral chemistry and proportional formulae for main minerals and major accessory phases in albitites, from EPMA data

	albite	oligoclase	microcline		Fe-CHL**	Mg-CHL**		T_{nw}	T_{rel}		AL_1	AL_2	Ep_1	Ep_2
	1)	2)	3)											
SiO_2	67.7	65.88	64.66	SiO_2	25.46	27.51	SiO_2	29.65	29.32	SiO_2	31.81	32.64	36.17	38.03
TiO_2	0.02	0.02	0.01	TiO_2	0.02	-	TiO_2	34.67	34.63	TiO_2	0.08	0.02	0.02	-
Al_2O_3	19.61	21.77	18.33	Al_2O_3	21.51	22.75	Al_2O_3	2.92	2.90	Al_2O_3	21.43	23.65	23.62	30.51
FeO*	-	-	-	Fe_2O_3	-	1.33	FeO*	0.23	0.76	FeO*	9.02	7.61	10.68	5.14
MnO	-	0.03	0.02	FeO	24.56	8.81	MnO	-	0.14	MnO	-	-	-	0.02
CaO	0.37	2.32	-	MnO	0.18	0.08	MgO	0.01	-	MgO	0.10	0.37	0.03	-
Na_2O	11.85	10.16	0.31	MgO	14.43	27.32	CaO	27.85	28.37	CaO	13.56	15.25	20.58	23.82
K_2O	0.05	0.03	16.83	CaO	0.11	0.05	Na_2O	0.02	-	La_2O_3	3.40	4.82	1.11	-
				Na_2O	-	-	Y_2O_3	1.31	0.07	Ce_2O_3	10.96	7.04	2.79	0.10
				K_2O	0.04	-	La_2O_3	-	-	Pr_2O_3	1.19	0.64	0.30	-
				H_2O*	11.47	12.38	Ce_2O_3	0.03	-	Nd_2O_3	4.08	2.59	1.21	-
							Pr_2O_3	0.05	-	Sm_2O_3	0.67	0.49	0.22	-
							Nd_2O_3	0.24	-	Gd_2O_3	-	0.16	0.12	-
							Sm_2O_3	0.19	-	Y_2O_3	0.07	0.27	0.06	-
							Gd_2O_3	0.21	-	ThO_2	-	0.19	0.22	-
Total	99.6	100.21	100.16	Total	97.78	100.24	Total	96.39	96.19	Total	96.37	95.74	97.13	97.62
Numbers of ions on the basis of 32(O)				*Numbers of ions on the basis of 28 (O)*			*Numbers of ions on the basis of 20 (O)*			*Numbers of ions on the basis of 12.5 (O)*				
Si	11.902	11.541	1.974	Si	5.464	5.314	Si	4.007	3.997	Si	2.932	2.911	2.976	2.929
Ti	0.003	0.003	0.001	Al^{IV}	2.536	2.686	Ti	3.523	3.550	Ti	0.006	0.001	0.001	-
Al	4.064	4.496	4.002	Al^{VI}	2.904	2.492	Al	0.465	0.466	Al^{IV}	0.068	0.089	0.024	0.071
Fe^{2+}	-	-	-	Ti	0.004	-	Fe^{2+}	0.012	0.039	Al^{VI}	2.261	2.398	2.268	2.699
Mn	-	0.004	0.003	Fe^{3+}	-	0.194	Mn	-	0.016	Fe^{3+}	0.110	0.157	0.571	0.369
Ca	0.07	0.435	-	Fe^{2+}	4.408	1.424	Mg	0.002	-	Fe^{2+}	0.585	0.410	0.164	-
Na	4.039	3.451	0.111	Mn	0.032	0.014	Ca	4.032	4.072	Mn	-	-	-	0.001
K	0.011	0.007	3.976	Mg	4.616	7.866	Na	0.006	-	Mg	0.013	0.049	0.004	-
				Ca	0.026	0.010								
Ab	98.04	88.64	2.72	Na	-	-	Y^{3+}	0.094	0.005	Sum (M)	3.043	3.104	3.032	3.140
An	1.69	11.19	-	K	0.010	-								
Or	0.3	0.19	97.28	(OH)	16.000	16.000	Sum (REE)	0.034	-	Ca	1.339	1.457	1.814	1.966
										Y^{3+}	0.004	0.013	0.003	-
							Ca site	4.072	4.160	Th^{4+}	-	0.004	0.004	-
							Ti site	4.002	4.055	Sum (REE)	0.681	0.511	0.172	0.003
Cations	20.089	19.937	20.068	Cations	20.000	20.000	Cations	12.176	12.217	Sum (A)	2.024	1.985	1.993	1.969

T_{nw} Newly formed REE-bearing titanite, T_{rel} relic REE-free titanite, *Fe-CHL* Fe-bearing chlorite, *Mg-CHL* Mg-bearing chlorite, AL_1 and AL_2 two generations of newly formed allanites, Ep_1 and Ep_2 two generations of newly formed REE-bearing epidote and REE-free epidote, respectively (see Fig. 5a). *Total iron as FeO; H_2O* was calculated using MINFILE program (Afifi and Essene 1988); **data from Carcangiu et al. 1997

$^{146}Nd/^{144}Nd$ normalized to 0.7219. Total procedural blanks were below 2 ng Sr and below 1 ng Nd and Sm. Rb–Sr and Sm–Nd isochrons were calculated using values of $\lambda_{Sr} = 1.42 \times 10^{-11}/\text{year}$ and $\lambda_{Sm} = 6.54 \times 10^{-12}/\text{year}$, respectively. Isochrons were calculated using the regression program of ISOPLOT version 2.82 (Ludwig 1995) taking into account 3 and 0.02% errors (2σ) in $^{87}Rb/^{86}Sr$, $^{147}Sm/^{144}Nd$ and $^{87}Sr/^{86}Sr$, $^{143}Nd/^{144}Nd$, respectively.

Results

Mineral chemistry in albitite

Mineral chemistry data for albitite are reported in Table 2. The chemical composition of plagioclase ranges from albite to oligoclase (analyses 1 and 2). Analyses performed on relic microcline indicate a fairly homogeneous composition, exemplified by analysis 3.

Newly formed chlorite shows a large compositional range from Fe^{2+}- to Mg-rich terms; REE are systematically below the detection limit of the microprobe. Epidote, the only LREE-bearing mineral identified, shows a complete solid solution ranging from REE-free epidote to Ce-allanite end-members. Integrated EPMA and SEM observations (Fig. 5 a,b) show a random distribution of REE within epidotes. This gives rise to typical patchy zoning, corresponding to a great variety of chemical compositions. Relic titanite is REE-free, while newly formed titanite contains Y+HREE. They probably substitute partially for Ca and Ti via the mechanism described by Green and Pearson (1986): $Ca^{2+} + Ti^{4+} \rightarrow (REE + Y)^{3+} + (Al, Fe)^{3+}$.

Whole-rock chemistry

Table 3 shows major- and trace-element contents in 24 representative samples, grouped according to the petrographic type. However, some albitized granitoid and albitite samples show intermediate characteristics between these two rock types, and thus, their assignation to either group is uncertain.

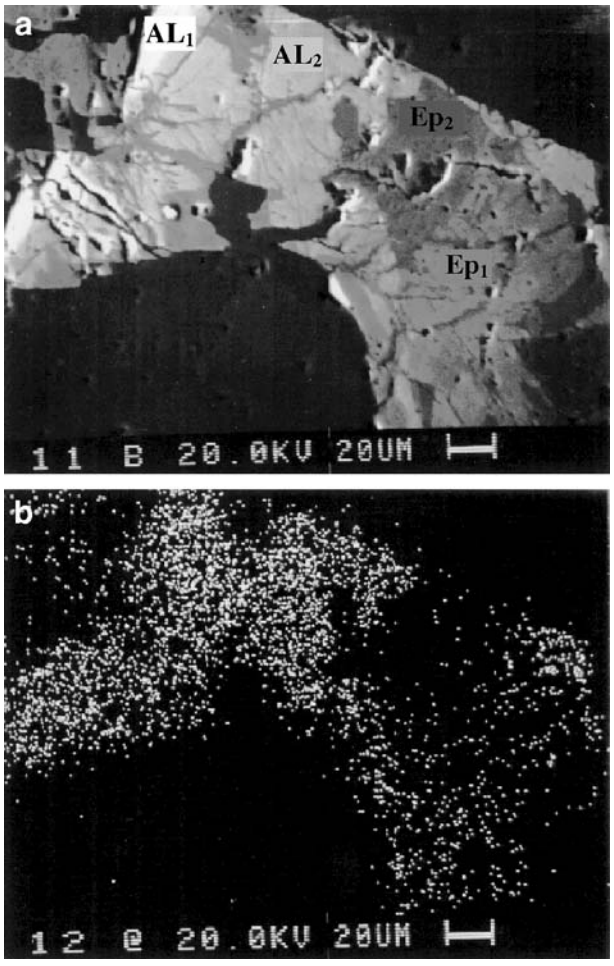

Fig. 5 **a** Photomicrograph showing random distribution of REE in a typical patchy-zoned epidote crystal in albitite (back-scattered electron image, from Bornioli et al. 1997). Using a gray scale mode, LREE contents are higher in the lighter zones than in the darker ones. Legend: AL_1 and AL_2 two successive generations of newly formed allanite; Ep_1 and Ep_2 two successive generations of epidote (REE-bearing and REE-free epidote, respectively) (see Table 2); **b** map of $Ce_{K\alpha}$ in the area of photomicrograph a)

Changes in rock volume with respect to the unaltered granitoid may have occurred during metasomatism in albitized rocks, especially in albitite. Therefore, to quantify mass fluxes, gains and losses by fluid–rock interaction were evaluated using the isocon diagram of Grant (1986), as modified by Petersson and Eliasson (1997). In Fig. 6, we compare the average compositions of albitites and unaltered granitoids. Following Baumgartner and Olsen (1995), the average composition was chosen to construct the plot, instead of the chemical composition of selected freshest samples (Leitch and Lentz 1994). We do not consider in this study albitized granitoids, because they show large variable chemical composition and wide standard deviations. MnO, Rb, and Ni are strongly depleted in albitite with respect to unaltered granitoid and often below the detection limits (d.l.) (Table 3). They are not shown in Fig. 6. Figure 6 clearly shows that albitization was accompanied by a net increase in Na_2O and depletion, to variable extent, in Fe_2O_{3total}, K_2O, MgO, Ba, Pb, Zn, and V. In contrast, SiO_2, TiO_2, and Th were typically immobile. Al_2O_3 and Sr show a slight enrichment, whereas, data points for CaO, P_2O_5, Y, Zr, Nb, and U suggest, within uncertainty limits, a nearly immobile behavior.

The REE patterns are presented in Fig. 7. All rocks show roughly comparable heavy rare-element contents (HREE). Moreover, while unaltered granitoids are generally characterized by major LREE enrichment (Fig. 7a) ($(La/Sm)_n = 3.01 - 7.4$), albitized granitoids (Fig. 7b) and albitites (Fig. 7c) display more variable spectra of LREE and MREE concentrations ($(La/Sm)_n = 0.16 - 6.25$). Their abundance is scattered, and sometimes lower than in unaltered granitoids. The Eu anomaly of unaltered granitoids is negative (Eu/Eu* from 0.26 to 0.85); values show lower scattering than those of albitized rocks (Eu/Eu* from 0 to 0.92) and albitites (Eu/Eu* from 0 to 0.99). However, the modified isocon Grant's diagram (Fig. 8), which reports the REE averages and 1σ uncertainty bars, shows that all REE were substantially immobile at the deposit scale, except Eu, which was lost to some extent from the albitized rocks.

Sr–Nd isotope ratios

Table 4 shows the Sr and Nd isotopic ratios of selected rocks.

The unaltered granitoids display Sr-isotope ratios between 0.714623 and 0.740157, while ranges for albitized granitoid and albitite are 0.711844–0.713841 and 0.713055–0.713844, respectively.

Nd-isotope ratios overlap: 0.512098–0.512248, 0.512080–0.512398 and 0.512149–0.512462 for unaltered granitoid, albitized granitoid, and albitite, respectively.

Discussion

Mineral chemistry in albitite

The complex composition of newly formed minerals reflects fluid–rock interaction during albitization. The REE, once mobilized from plagioclase and allanite during the metasomatic stage, were partitioned into newly formed epidote, according to the scheme of Pan and Fleet (1991). The patchy zone texture, observed within the epidote crystals, suggests that the process occurred in different stages. In

Table 3 Major (wt%) and trace (ppm) elements of selected samples of unaltered granitoids, albitized granitoids and albitites from central Sardinia

Unaltered granitoids								Albitize granitoids								Albitites								
								XRF analyses																
Sample	Abo15	Abo19	Alb21	Abo31	Alb40	Alb56	Alb 84	Alb1b	Abo11	Abo18	Abo24	Alb27	Alb30	Alb31	Alb66	Abo8	Alb15	Alb16	Alb28	Alb34	Alb44	Alb64	Alb79	Alb80
SiO_2	70.44	69.05	71.23	65.44	71.27	67.56	74.27	61.16	69.41	72.84	68.83	71.00	63.12	69.22	71.23	68.52	68.64	67.69	69.20	71.23	67.21	67.20	67.21	67.50
TiO_2	0.44	0.49	0.22	0.56	0.24	0.36	0.14	0.37	0.61	0.10	0.32	0.53	1.01	0.21	0.35	0.18	0.20	0.34	0.10	0.10	0.40	0.31	0.45	0.68
Al_2O_3	15.40	14.99	15.36	16.98	14.80	15.80	13.29	22.70	16.07	16.31	16.68	15.89	20.71	18.12	15.36	18.87	17.96	18.63	18.62	17.11	19.29	19.14	19.12	18.94
$Fe_2O_{3\ tot.}$	2.78	3.73	1.83	4.66	2.40	2.75	1.81	0.25	0.22	0.10	0.19	0.92	0.49	0.26	0.68	0.11	0.33	0.17	0.05	0.17	0.29	0.12	0.08	0.04
MnO	0.04	0.08	0.01	0.09	0.06	0.06	0.03	0.01	0.01	0.01	0.01	0.01	0.01	0.01	0.01	0.01	0.01	0.01	0.01	0.01	0.01	0.01	0.01	0.00
MgO	0.74	1.19	0.67	0.96	0.57	0.97	0.27	2.03	3.26	0.10	3.93	0.18	0.69	0.38	2.07	0.03	0.25	0.22	0.02	0.10	0.20	0.64	0.07	0.04
CaO	1.72	3.02	2.62	3.30	1.64	1.27	1.43	4.28	0.89	2.45	0.35	4.29	3.81	2.39	0.63	1.87	2.36	2.07	1.91	1.46	1.16	0.75	1.15	0.75
Na_2O	3.10	2.92	3.21	3.97	3.84	3.04	3.52	7.83	8.49	7.35	8.33	5.93	8.65	8.87	8.63	10.03	9.68	10.29	9.80	9.36	10.73	11.30	11.57	11.62
K_2O	4.24	3.93	4.35	3.25	4.81	6.94	4.44	0.16	0.05	0.17	0.07	0.17	0.47	0.13	0.07	0.14	0.08	0.05	0.09	0.12	0.18	0.10	0.05	0.04
P_2O_5	0.28	0.15	0.08	0.20	0.07	0.20	0.05	0.16	0.17	0.18	0.05	0.20	0.20	0.10	0.18	0.01	0.10	0.22	0.05	0.06	0.06	0.13	0.00	0.04
LOI	0.83	0.45	0.42	0.59	0.29	1.05	0.75	1.06	0.81	0.37	1.22	0.88	0.85	0.32	0.80	0.24	0.41	0.31	0.15	0.28	0.46	0.31	0.30	0.33
Total	100.01	100.00	100.00	100.00	99.99	100.00	100.00	100.01	99.99	99.98	99.98	100.00	100.01	100.01	100.01	100.01	100.02	100.00	99.99	100.00	99.99	100.01	100.01	99.98
Rb	165	111	77	126	200	204	72	nd	nd	3	nd	2	18	nd	nd	nd	nd	nd	nd	nd	nd	nd	nd	nd
Sr	188	159	218	199	76	193	128	1006	119	376	50	546	848	481	66	212	340	509	454	340	122	117	182	146
Ba	815	796	983	976	446	1382	823	68	35	32	25	100	106	66	42	29	59	nd	64	51	47	46	67	63
Zr	178	139	148	315	126	221	115	167	191	148	279	355	270	158	202	197	168	227	207	127	247	218	263	316
Nb	15	12	5	14	18	7	Nd	16	13	nd	10	21	19	15	18	nd	11	8	7	8	14	22	26	29
Zn	79	71	7	72	53	54	16	nd	nd	1	nd	7	nd	nd	2	nd	nd	nd	nd	nd	4	2	1	nd
Pb	26	28	22	21	34	52	23	nd	nd	10	10	25	nd	nd	nd	nd	nd	nd	nd	nd	7	15	nd	8
Ni	5	6	nd	3	nd	nd	Nd	4	nd	2	4	nd	6	2	nd	nd	nd	nd	nd	nd	nd	nd	nd	nd
Cr	Nd	nd	nd	nd	nd	nd	Nd	nd	nd	nd	nd	nd	94	nd	nd	nd	nd	nd	nd	nd	nd	nd	nd	nd
V	23	52	15	41	18	30	13	27	29	10	26	28	90	15	25	10	18	21	9	13	14	14	17	21
Y	13	18	9	28	11	33	17	7	3	33	9	24	36	7	13	8	28	16	9	17	7	25	16	30
												ICP-MS analyses												
La	39.8	48.3	49.3	90.8	32.1	48.4	25.0	1.4	2.1		3.3	95.8	49.2		1.7	82.7	56.0	44.5	8.1	38.3	8.3	1.6	3.5	1.4
Ce	83.5	101.0	93.4	173.0	68.9	95.1	54.9	4.6	4.6		8.4	174.0	105.0		3.1	198.0	122.0	91.5	17.2	85.0	20.0	4.2	9.0	5.5
Pr	9.7	11.7	8.8	18.5	8.4	10.3	5.9	1.2	0.8		1.0	18.7	12.0		0.6	23.0	13.2	10.3	2.3	10.4	2.5	0.8	1.4	1.6
Nd	37.6	45.6	31.0	66.2	34.5	44.9	23.4	1.0	4.2		4.8	67.3	46.6		3.4	87.6	49.3	40.4	10.5	43.2	10.4	3.6	6.5	10.9
Sm	7.8	9.8	4.3	11.1	7.0	8.0	4.1	1.8	1.4		1.5	9.9	9.0		1.1	14.5	9.6	6.3	1.6	7.8	2.0	0.8	2.4	5.7
Eu	1.4	1.7	0.8	1.6	0.5	1.0	1.0	0.5	0.4		0.3	1.4	1.6		nd	1.1	nd	1.7	0.3	0.7	0.1	0.1	0.2	0.6
Gd	6.0	7.1	2.7	9.1	5.3	7.1	3.1	1.8	1.2		1.7	6.1	7.9		1.6	6.1	7.3	3.7	1.6	5.6	1.4	2.5	3.0	6.5
Tb	0.7	0.9	0.3	1.1	0.7	1.1	0.6	0.3	0.2		0.3	0.9	1.2		0.4	0.6	1.0	0.6	0.2	0.7	0.3	0.7	0.5	1.1
Dy	3.1	4.3	2.3	6.0	3.7	6.4	3.7	2.0	1.2		1.6	5.1	7.2		2.4	2.7	6.1	3.8	1.5	4.0	1.6	5.0	3.6	5.9
Ho	0.4	0.7	0.4	1.1	0.5	1.2	0.8	0.5	0.3		0.3	1.0	1.4		0.5	0.5	1.2	0.8	0.4	0.8	0.4	1.2	0.7	1.1
Er	1.1	1.7	0.9	3.2	1.5	2.9	2.5	1.1	0.9		0.9	2.8	4.4		1.7	1.4	2.7	2.4	1.4	1.6	0.9	3.6	2.3	2.9
Tm	0.1	0.2	0.1	0.4	0.2	0.5	0.3	0.3	0.3		0.1	0.3	0.6		0.3	0.3	0.4	0.4	0.2	0.3	0.2	0.6	0.4	0.4
Yb	0.8	1.4	0.7	3.0	1.0	2.2	1.9	1.2	0.9		1.1	1.7	3.4		1.2	1.2	2.3	2.1	1.4	1.7	0.9	3.3	1.8	2.5
Lu	0.1	0.1	0.1	0.5	0.2	0.3	0.3	0.3	0.2		0.2	0.2	0.5		0.2	0.3	0.3	0.4	0.2	0.3	0.1	0.5	0.3	0.4
Th	11.3	10.8	19.3	18.2	19.3	23.2	14.7	8.2	22.5		8.5	31.7	14.5		31.5	57.9	43.9	32.2	8.3	14.6	16.7	13.0	9.3	28.0
U	2.5	3.2	1.3	2.4	2.3	3.3	0.6	1.1	0.7		1.1	2.9	2.9		1.5	1.4	4.2	2.3	0.7	1.6	0.5	0.9	0.4	2.4
(Eu/Eu*)n	0.61	0.60	0.64	0.48	0.26	0.40	0.86	0.92	0.89		0.58	0.50	0.59		0.00	0.31	0.00	0.99	0.54	0.31	0.11	0.14	0.18	0.31

(Eu/Eu)n* Eu anomaly expressed as ratio of measured normalized Eu and interpolated normalized Eu*, *nd* below detection limit

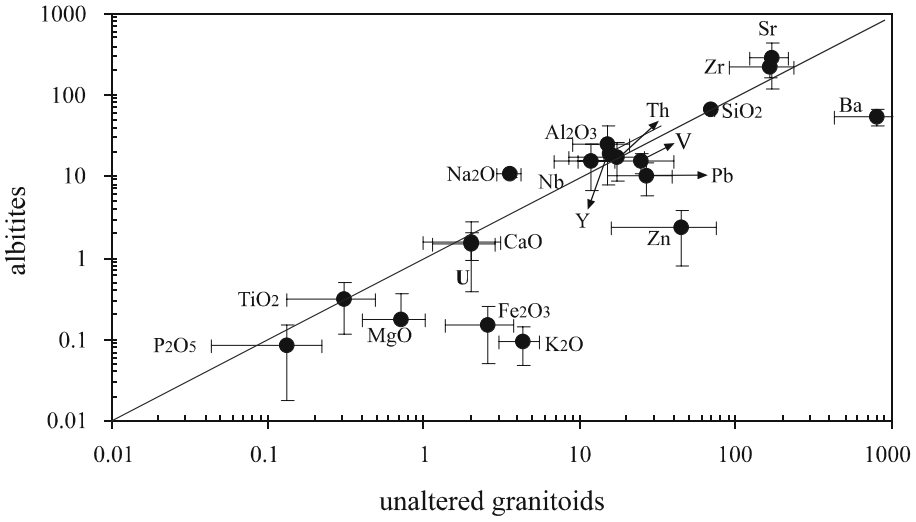

Fig. 6 Unaltered granitoid vs. albitite log–log isocon diagram (after Grant 1986), for major and trace elements. Data for major elements are plotted in wt%, and for trace elements in ppm. *Error bars* are 1σ standard deviation. Average elemental concentrations (cf., Baumgartner and Olsen 1995) of rocks are plotted. *Diagonal line*: points where elemental concentrations in albitites equal elemental concentrations in unaltered granitoids

particular, application of the chemical criterion proposed by Tulloch (1979) (Carcangiu et al. 1997), indicates that most of newly formed epidotes originated by alteration of plagioclase, and only a few crystals replace magmatic allanite.

Whole-rock chemistry

Table 3 shows that albitized granitoids exhibit more compositional scatter than albitites. Indeed, albitized granitoids represent intermediate steps of the alteration process, corresponding to various degrees of water–rock interaction. The incompleteness of alteration processes in the albitized granitoids is proven, for instance, by the gradual replacing of potassium feldspar by albite, which preserves the general shape and twin plane of the original alkali feldspar (Morad et al. 1990; Slaby 1992). In contrast, the smaller scatter of data in albitites suggests an approach to chemical equilibrium operated by higher fluid/rock ratios.

The significant loss of K, Rb, Ba, and Pb observed in albitite, with respect to unaltered granitoid, is explained by dissolution of potassium feldspar and biotite during albitization and the lack of suitable newly formed minerals to accommodate such elements. Likewise, the breakdown of biotite and other mafic minerals accounts for the almost total removal of Fe, Mg, Mn, Zn, Ni, and V from albitite. The released Fe and Mg were partially re-accommodated in the lattice of newly formed Fe-bearing minerals (e.g., hematite, epidote) and in Mg-bearing minerals (e.g., chlorites, from clinochlore to chamosite), and partially removed from the system. The immobility of Si and Al during albitization of the granitoids is consistent with the substitution of albite for potassium feldspar and, subordinately, Ca-bearing plagioclase. The substantial immobility of Ca and Sr is explained by the fact that these elements, released from alteration of feldspars, were essentially partitioned into newly formed Ca-epidote and/or albite. Especially, acidic plagioclase is suitable to accommodate Sr, because of its large partition coefficient (Arth 1976).

The immobility of TiO_2 is consistent with the stability of magmatic titanite during alteration, as indicated by textural evidence, and partition of Ti released from igneous biotite into newly formed titanite. Y was immobile because any amount that might have partially been leached from primary allanite and titanite, was rearranged in the lattice of newly formed titanite and epidote. Zircon was stable during albitization, thus accounting for the substantial immobility of Zr. U and Th were relatively immobile, although leaching of allanite, which may be considered the main U–Th holder in the granitoids, released these elements, which were, however, partitioned into newly formed allanite-Ce. Unlike the above elements, Na was added to albitized rocks, suggesting that the fluids were relatively Na-rich, i.e., they had a Na/K ratio significantly higher than 1 (Orville 1963, 1972).

The quite uniform LREE pattern exhibited by unaltered granitoid (Fig. 7a), compared with the variable patterns of albitized rocks (Fig. 7b,c), suggests significant mobilization of LREE during albitization. This likely resulted from dissolution of metamict allanite (up to 1% in modal proportion in unaltered granitoid, virtually absent in albitized rocks), the only mineral with LREE contents higher than EPMA detection limits. However, as leached LREE were partitioned into newly formed epidote (Carcangiu et al. 1997), this explains why LREE were, on average, immobile at the deposit scale (Fig. 8). Moreover, the scattered REE patterns of albitite, compared with the uniform pattern of unaltered granitoid, suggest that albitization was operated by non-magmatic fluids.

Hydrothermal fluids generally contain low absolute REE concentrations; thus, the difference in REE content that arises from hydrothermal fluid–rock interaction is, usually, too small to be detectable on REE-chondrite normalized patterns (Bau 1991). Hence, the variable REE patterns observed in Fig. 7 suggest that the water/rock ratio was high, probably larger than 100. In other words, albitization occurred in an extremely fluid-dominated system, where the REE patterns are significantly changed by the precipitation of minerals characterized by high mineral/liquid partition

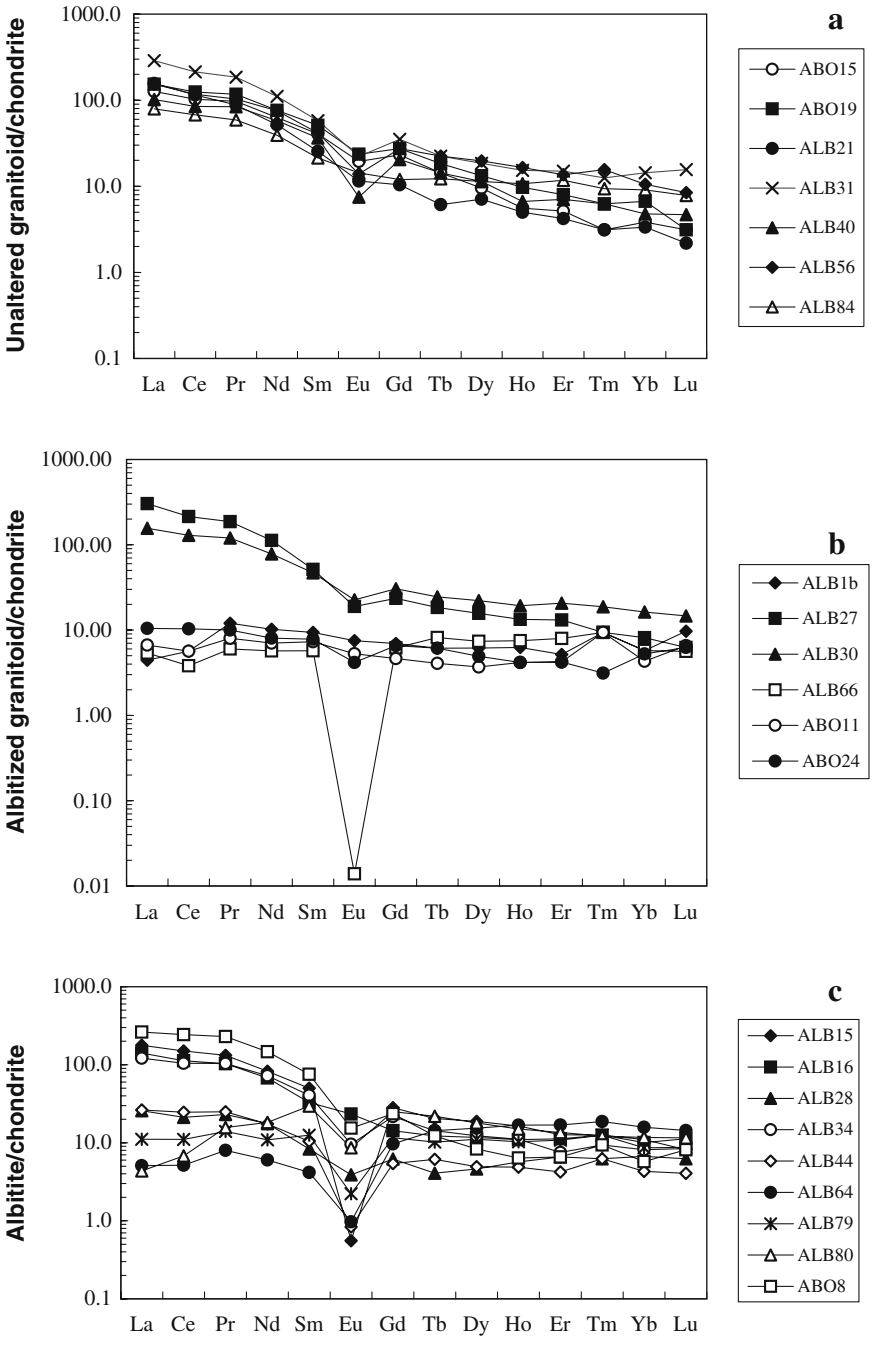

Fig. 7 Chondrite-normalized REE diagrams (after Sun and Mc Donough 1989) for unaltered granitoid (**a**), albitized granitoid (**b**), and albitite (**c**)

coefficients. Eu depletion in the albitite, with respect to unaltered granitoid (Fig. 8), indicates that, because Eu is mobile as Eu^{2+}, the reduced Eu present in magmatic feldspars was mobilized and lost, to some extent, to the fluids during feldspar transformation into albite.

The pH of the fluids may be estimated by considering the mineral paragenesis of albitized rocks. The replacement of potassium feldspar by albite, and the occurrence of rare muscovite with quartz, indicate nearly neutral to slightly alkaline pH (Montoya and Hemley 1975). This is consistent with the substantial immobility of Al, and suggests a relatively low temperature of the fluids (e.g., Charoy and Pollard 1989). The fluids evolved from reduced to oxidized through time, as newly formed epidote and hematite contain Fe^{3+}. However, in the alteration areas where chlorite occurs and epidote is absent, the fluids may have been oxidized to a lesser extent. Lastly, the fluids were relatively rich in complexing agents, as indicated by LREE mobilization from primary minerals of the granitoids (Schade et al. 1989).

However, complexing agents such as CO_2, F, and H_2S were probably not significant, because carbonates, fluorides, and sulfides do not occur in albitized rocks, although the physical–chemical conditions (pH, T) of the fluids were favorable to their deposition (Bornioli et al. 1996). In contrast, Cl was probably a major component (Bornioli et al. 1997), as Cl-rich fluids preferentially mobilize LREE

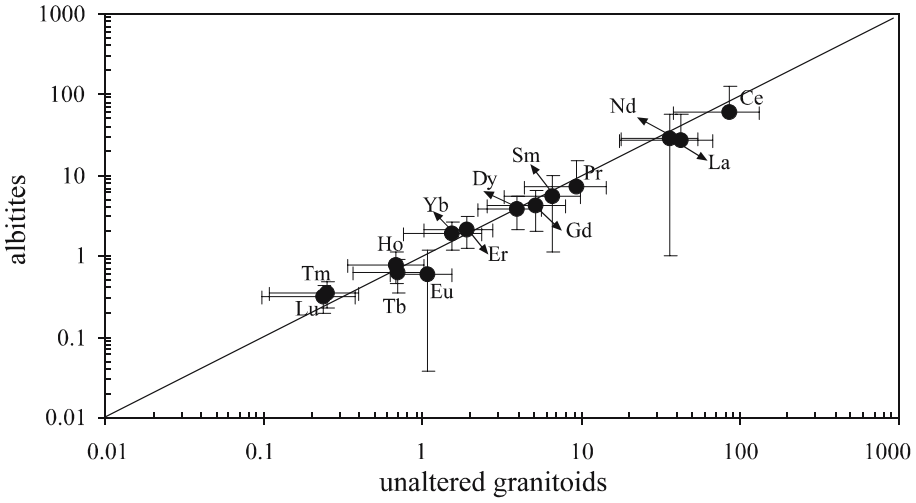

Fig. 8 Unaltered granitoid vs. albitite log–log isocon diagram (after Grant 1986), for REE elements (ppm). Average REE concentrations of rocks are plotted (cf., Baumgartner and Olsen 1995). *Error bars* are 1σ standard deviation. *Diagonal line*: points where REE concentrations in albitites equal REE concentrations in unaltered granitoids

(e.g., Taylor and Fryer 1983; Wood 1990a, b). The presence of Na–Cl-rich fluids may suggest the participation of seawater, probably chemically modified by interaction with the metasedimentary basement in the albitization process.

Newly formed paragenesis and alteration stages

After granitoid emplacement, three alteration stages, each characterized by a typical mineral assemblage, were recognized (Fig. 9):

1) an *early prograde stage*, during which albitization was locally associated with chloritization, involving release of SiO_2, and epidotization, together with minor dissolution and re-precipitation of quartz. The vugs formed by quartz leaching, and fractures originating from cooling of the pluton, enhanced rock permeability, favoring the circulation of fluids within the granitoids. The magmatic texture of unaltered granitoid was preserved;
2) a *late prograde stage*, characterized by increasing alteration, and obliteration of the original textures of the protolith;
3) a *retrograde alteration stage*, during which the newly formed minerals filled vugs and veinlets crosscutting the rocks.

Sr–Nd isotope systematics

In the $^{87}Sr/^{86}Sr$ vs $^{87}Rb/^{86}Sr$ isochron diagram (not shown here), the Rb–Sr system does not yield any isochron for the unaltered granitoids; however, the best fit line to data points corresponds to an age of 274±29 Ma, with an associated MSWD of 14.1. Both the age and the initial Sr-isotope ratio (0.710638±0.00031) associated with the regression line fall into the published ranges of late-Variscan granitoids from Sardinia (Tommasini et al. 1995).

Because of the very low to nil Rb contents in albitized granitoids and albitites, the Rb–Sr system does not allow to obtain any isochron and, thus, no age is determined for albitization. Nevertheless, the Sr-isotope data allow us to set constraints on a possible age for such a process. In this view, we consider that albitization might have taken place during the emplacement of either Variscan granitoids, or Tertiary ignimbrites, i.e., about 274 or 21 Ma ago, respectively (Table 4). These two events are, in fact, the only ones when there was enough supply of heat to trigger a hydrothermal circulation of fluids in this area.

In principle, we must consider the hypothesis that granitoid albitization could be related with Tertiary hydrothermal circulation through the granitoids bordering the rift margin. In this case, the range of Sr-isotope ratios of albitites should overlap to a great extent with the range of unaltered granitoids (0.7146–0.7402), because of similar isotopic evolution by ^{87}Rb decay into ^{87}Sr since 274 Ma. This is not supported by the data of albitites, which display lower Sr isotope ratios than unaltered granitoids. Moreover, because albitized granitoid is a transitional rock between unaltered granitoid and albitite, it should exhibit intermediate Sr-isotope composition between the two end-members. Actually, at 21 Ma albitized granitoids would display even lower or at least similar Sr-isotope ratios to albitites. Therefore, we believe that the hypothesis of a Tertiary age for albitization is not viable, and we suggest that albitization must be a process shortly postdating the granitoid emplacement.

Nd-isotope data do not define any isochron for unaltered granitoids, albitized granitoids, and albitites in the $^{147}Sm/^{144}Nd$ vs $^{143}Nd/^{144}Nd$ plot (Fig. 10). Thus, no age information can be obtained with the Sm/Nd system. However, the fact that most samples lie close to the reference isochron of 274±29 Ma in the plot supports that

Table 4 Sr and Nd isotopic ratios in selected rock samples

Sample	Rb (ppm)	Sr (ppm)	$^{87}Rb/^{86}Sr$	$^{87}Sr/^{86}Sr$	Sm (ppm)	Nd (ppm)	$^{147}Sm/^{144}Nd$	$^{143}Nd/^{144}Nd$	$^{143}Nd/^{144}Nd_{(274Ma)}$	$\varepsilon_{Nd(274Ma)}$
Granitoids										
Abo15	165	188	2.529	0.720980(10)	7.8	37.6	0.125	0.512202(12)	0.51198	−5.99
Abo19	111	159	2.029	0.718821(8)	9.8	45.6	0.130	0.512248(8)	0.51201	−5.27
Alb21	77	218	1.026	0.714623(7)	4.9	31	0.095	0.512098(10)	0.51193	−6.95
Alb21 replicate[a]	75.85	216.7	1.014	0.714616(10)	5.14	31.92	0.097	0.512103(7)	0.51193	−7.00
Abo31	126	199	1.823	0.717772(10)	11.1	66.2	0.101	0.512133(9)	0.51195	−6.48
Alb40	200	76	7.615	0.740157(13)	7	34.5	0.122	0.512196(10)	0.51198	−6.00
Abo40 replicate[a]	202.62	77.03	7.611	0.740172(11)	7.32	35.98	0.123	0.512197(9)	0.51198	−6.00
Alb56	204	193	3.056	0.721252(6)	8	44.9	0.107	0.512174(17)	0.51198	−5.89
Alb84	106	49	6.187	0.735181(10)	4.1	23.4	0.105	0.512142(8)	0.51195	−6.45
Albitized granitoids										
Alb1b		1006		0.711844(7)	1.8	6.1	0.178	0.512186(28)	0.51187	−8.17
Alb1b replicate[a]	0.23	1008.25		0.711836(12)	1.76	5.94	0.1786	0.512188(9)	0.51187	−8.18
Abo11		119		0.712872(9)	1.4	4.2	0.201	0.512398(8)	0.51204	−4.86
Abo18	3.00	376	0.02	0.712079(5)	15	88	0.103	0.512121(12)	0.51194	−6.79
Abo24		50		0.713110(7)	1.5	4.8	0.188	0.512133(4)	0.51180	−9.56
Alb27	2.00	546	0.01	0.713572(9)	9.9	67.3	0.088	0.512125(8)	0.51197	−6.16
Alb27 replicate[a]	1.86	547.81	0.009	0.713569(13)	10.21	68.03	0.0904	0.512128(11)	0.51197	−6.19
Alb30	10.00	848	0.03	0.713841(6)	9	46.6	0.116	0.512080(7)	0.51192	−8.05
Alb31		481		0.713769(6)	4.2	23.3	0.109	0.512157(9)	0.51196	−6.30
Alb66		66		0.712826(8)	1.1	3.4	0.195	0.512364(6)	0.51201	−5.33
Alb66 replicate[a]	0.081	64.87	0.0036	0.712830(9)	1.32	4.08	0.195	0.512370(8)	0.51202	−5.21
Albitites										
Abo8		212		0.713801(8)	14.5	87.6	0.100	0.512151(8)	0.51197	−6.09
Alb15		340		0.713862(5)	9.6	49.3	0.117	0.512172(7)	0.51196	−6.29
Alb16		509		0.713109(7)	6.3	40.4	0.094	0.512149(9)	0.51198	−5.92
Alb16 replicate[a]	0.002	511.01		0.713098(15)	5.99	39.84	0.091	0.512151(7)	0.51199	−5.77
Alb28		454		0.713610(4)	1.6	10.5	0.092	0.512200(9)	0.51203	−4.85
Alb34		340		0.713844(9)	7.8	43.2	0.109	0.512153(6)	0.51196	−6.37
Alb44		122		0.713798(13)	2	10.4	0.116	0.512162(6)	0.51195	−6.45
Alb64		117		0.713055(5)	0.8	3.6	0.134	0.512165(17)	0.51192	−7.03
Alb64 replicate[a]		114.14		0.713071(18)	0.91	4.09	0.1342	0.512155(11)	0.51191	−7.24
Alb79		182		0.713252(10)	2.4	6.5	0.222	0.512432(10)	0.51203	−4.97
Alb80		146		0.713769(6)	5.7	10.9	0.315	0.512462(16)	0.51190	−7.71
Alb80 replicate[a]	0.011	149.32	0.0002	0.713771(19)	4.67	8.97	0.3137	0.512455(9)	0.51189	−7.80
Representative rocks of basement										
MB[b]	118.4	192.6	1.779	0.72391	7.86	38.28	0.124	0.51186		−7.95
Representative volcanic rocks										
Rhyolites[c]	427.5	268.2	4.613	0.70631				0.51245		

ε_{Nd} was calculated using the following present-day values for CHUR: $^{147}Sm/^{144}Nd=0.1967$; $^{143}Nd/^{144}Nd=0.512640$; $\lambda^{147}Sm=6.54\times10^{-12}$ a^{-1}

[a]Rb, Sr, Sm and Nd concentrations determined by ID-TIMS

[b]Average of ten analyses of low-grade metasedimentary rocks (metasandstones and metasiltstones as MB) outcropping close to the studied area (Castorina et al., unpublished data)

[c]Average of six analyses of fresh volcanic rocks outcropping in the northern part of the investigated area (Castorina et al., unpublished data)

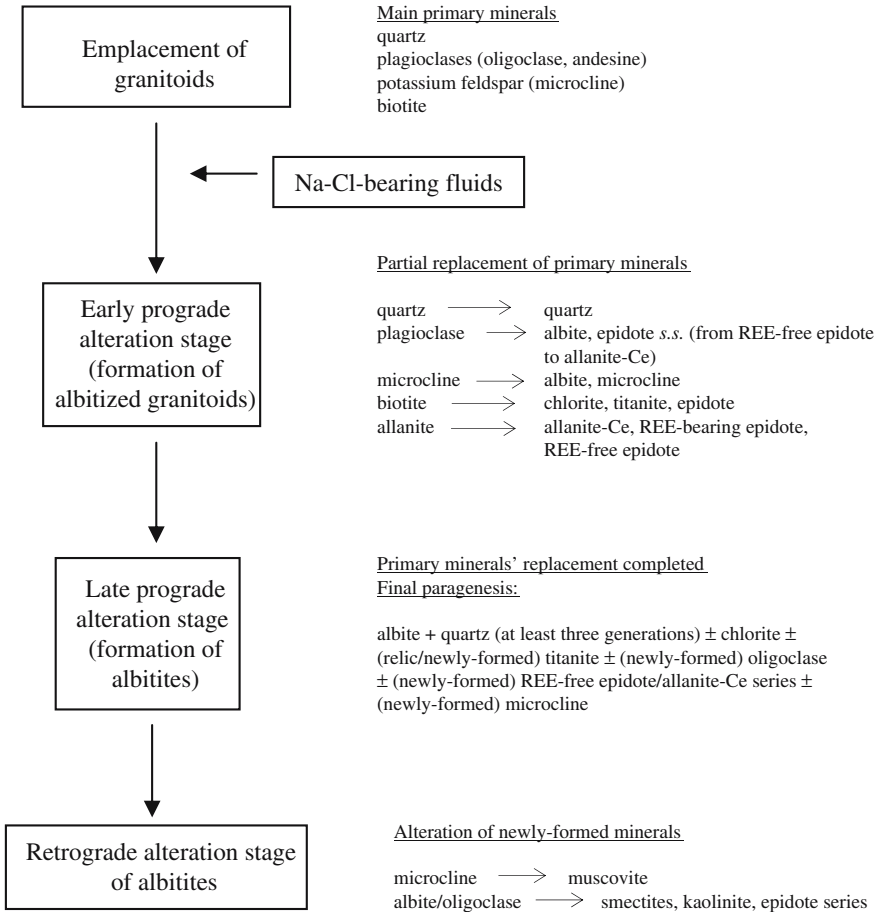

Fig. 9 Time-paragenesis diagram

albitization was connected to the granitoid emplacement. From Fig. 10 it is also apparent that some albitized granitoids lie farther off the reference isochron than the other samples, even taking into account the associate errors of the $^{147}Sm/^{144}Nd$ and $^{143}Nd/^{144}Nd$ ratios. This may be explained by the fact that the albitized granitoids do not represent isotopically closed systems because of incomplete reactions between minerals and fluids, as observed in thin sections.

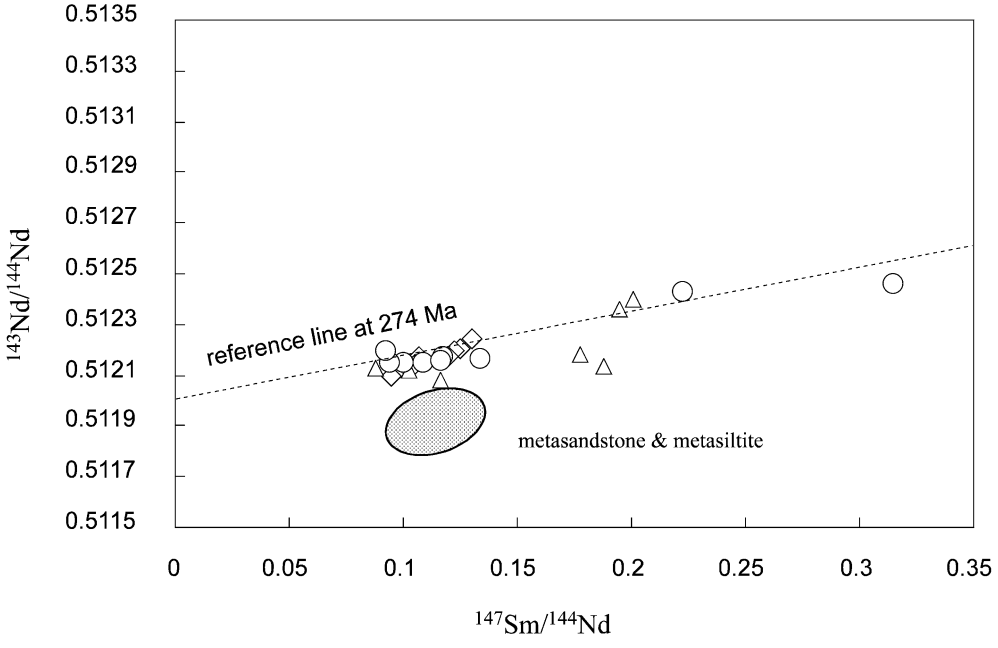

Fig. 10 Plot of measured $^{147}Sm/^{144}Nd$ ratios vs. $^{143}Nd/^{144}Nd$ ratios for unaltered granitoids (*diamonds*), albitized granitoids (*triangles*) and albitites (*circles*). Also shown is the field of non-carbonatic rocks of the basement

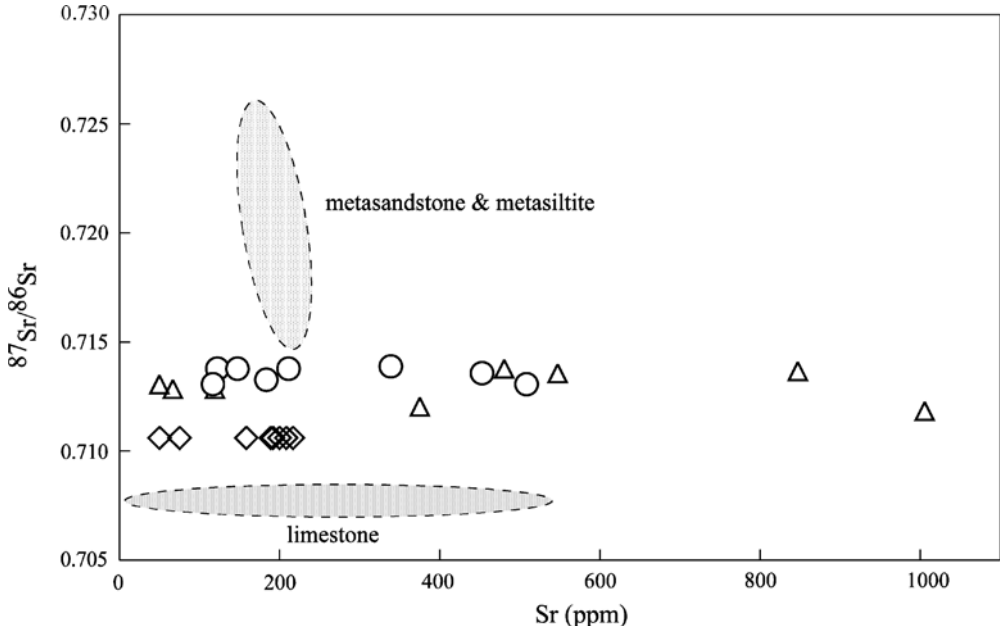

Fig. 11 Sr vs $^{87}Sr/^{86}Sr$ ratios calculated at 274 Ma for unaltered granitoids, albitized granitoids, and albitites (*symbols* as in Fig. 10). Also shown are the fields for metasandstones, metasiltites, and carbonatic rocks of the basement

The higher Sr-isotope ratios of albitized rocks, with respect to unaltered granitoids at 274 Ma, rule out that the albitizing fluids were of magmatic derivation. Such fluids acquired their Sr-isotope composition circulating through the metasedimentary basement intruded by the granitoids. In this view, as the average Sr-isotope ratios of non-carbonatic and carbonatic formations of the basement were about 0.720 (n=10), and 0.708 (n=10), respectively (Castorina, unpublished data), it is evident that the fluids were provided with Sr mainly by non-carbonatic rocks (Fig. 11). We can calculate the Sr contribution using the equation of Johnson and Mc Culloch (1995):

$$R_{alb} = \left[R_b C_b f + R_g C_g (1-f)\right] / \left[C_b f + C_g (1-f)\right] \quad (1)$$

where R_{alb} is average IR_{Sr} (initial ratio) of albitite (0.7133); R_g and R_b are average IR_{Sr} of unaltered granitoid (0.7106) and non-carbonatic rocks (0.720), respectively; C_g and C_b are average Sr concentrations in unaltered granitoid (161 ppm) and non-carbonatic rocks (160 ppm), and f represents Sr contribution (%) from non-carbonatic rocks to fluids. Solving Eq. 1 for f resulted in non-carbonatic rocks providing about 22 wt% of total Sr in albitite. In other words, the majority of Sr in albitites was inherited from the parent granitoids, in agreement with information provided by elemental Sr.

As regards Nd isotopes, from Fig. 10 it is evident that the Nd contribution from the non-carbonatic basement to the albitites was negligible. In fact, there is a general overlapping of the Nd-isotope ratios of albitized rocks and unaltered granitoids, which are significantly different from the Nd-isotope ratios of the basement rocks. This conclusion agrees with information provided by elemental Nd.

Conclusions

Albitites from central Sardinia were formed by fluids metasomatizing late-Variscan granitoids. Mineralogy and geochemical data suggest that albitization was accompanied by Na addition and leaching of K, Fe, Mg, and geochemically similar trace elements, mainly from potassium feldspar (replaced by albite) and biotite (breakdown). Ca, Ti, Si, Al, U, and HREE were substantially immobile during metasomatism, because, once leached from the magmatic minerals, they were accommodated in newly formed minerals. The LREE were largely variable at the sample scale in the albitized rocks, with respect to unaltered granitoids, but substantially immobile at the deposit scale; this suggests that the metasomatic fluids were not of magmatic derivation, as also supported by the higher Sr-isotope ratios of albitites with respect to the initial ratio of unaltered granitoids. The metasomatic fluids were slightly alkaline, mainly oxidized, relatively (Na)Cl-rich to mobilize mainly LREE. Probably, they contained little sulfur because of lack of sulfides and sulfates in the albitized rocks. The temperature probably was moderate to low, if epidote and chlorite crystallized almost contemporaneously with newly formed albite.

The Sr and Nd isotopes fail to date albitization. However, although a rigorous geochronological determination of the age of the albitites is not possible, coupling regional geological features with field and isotopic data, it is plausible to assign to this process an age close to the emplacement of the granitoids. Calculations suggest that about 22% of the radiogenic ^{87}Sr added to albitites by the fluids came by leaching non-carbonatic rocks of the pre-Variscan basement. In contrast, all Nd of albitites was inherited from the granitoids.

Acknowledgements This research was supported by the Consiglio Nazionale delle Ricerche, Istituto di Geologia Ambientale e Geoingegneria, Sections of Cagliari and Rome (*La Sapienza*), Italy, within the project *Minerali e rocce industriali: prospezione geomineraria*, *valorizzazione e caratterizzazione dei materiali*, and M.P.I. (60% grants to Prof. G. Padalino). We have benefited from constructive reviews by Albrecht von Quadt and Urs Schaltegger. The last version of this manuscript benefited from the constructive criticism and suggestions of Piero Lattanzi.

References

Abdalla HM, Ishihara S, Matsueda H, Abdel Monem AA (1996) On the albite-enriched granitoids at Um Ara area, southeastern desert, Egypt. 1. Geochemical, ore potentiality and fluid inclusion studies. J Geochem Explor 57:127–138

Afifi AM, Essene EJ (1988) *MINFILE*: A microcomputer program for storage and manipulation of chemical data on minerals. Am Mineral 73(3–4):446–448

Arth JG (1976) Behaviour of trace elements during magmatic processes—a summary of theoretical models and their applications. J Res US Geol Surv 4:41–47

Arthaud F, Matte PH (1975) Les décrochements tardi-hercyniens du Sud-ouest de l'Europe: Géometrie et essai de reconstitution des conditions de la déformation. Tectonophysics 25:139–171

Assorgia A, Barca S, Porcu A, Spano C, Balogh K, Rizzo R (1998) The Oligocene–Miocene sedimentary and volcanic successions of central Sardinia, Italy. Roman J Strat 78:9–23

Bachiller N, Casquet C, Galindo C, Quilez E (1997) Hydrothermal alterations in leucogranites from the Burguillos del Cerro intrusive complex (Badajoz, SW Spain). Evidence for the pulsatile mixing of igneous and meteoric fluids. In: Papunen (ed) Mineral deposits. Balkema, Rotterdam, pp 605–608

Bau M (1991) Rare-earth element mobility during hydrothermal and metamorphic fluid–rock interaction and the significance of the oxidation state of europium. Chem Geol 93:219–230

Baumgartner LP, Olsen SN (1995) A least-squares approach to mass transport calculations using the isocon method. Econ Geol 90:1261–1270

Bird DK, Norton DL (1981) Theoretical predictions of phase relations among aqueous solutions and minerals. Geochim Cosmochim Acta 45:1479–1493

Bornioli R, Carcangiu G, Palomba M, Peretti R, Tamanini M, Zucca A (1993) REE-mineralization in the albite deposit of Central Sardinia (Italy): Geological, mineralogical and petrological aspects, REE-bearing minerals. Proceedings of "Rare Earth Minerals: Chemistry, origin and ore deposits", London, April 1–2 1993, 15–17

Bornioli R, Fadda S, Fiori M, Grillo SM, Marini C (1996) Genetic aspects of albitite deposits from Central Sardinia: mineralogical and geochemical evidence. Explor Min Geol 5:61–72

Bornioli R, Carcangiu G, Palomba M, Simeone R, Tamanini M (1997) Rare earth elements in the albitites of Central Sardinia (Italy). Note I: the mineralization of Ottana. Per di Min 66:269–285

Bralia A, Ghezzo C, Guasparri G, Sabatini G (1982) Aspetti genetici del batolite sardo-corso. Rend Soc Ital Mineral Petrol 38:701–764

Carcangiu G, Palomba M, Tamanini M (1996) Allanite-(Ce) ed epidoti a terre rare nelle albititi della Sardegna Centrale (Italia). Mineral Petrogr Acta XXXVIII:1–11

Carcangiu G, Palomba M, Tamanini M (1997) REE-bearing minerals in the albitites of central Sardinia, Italy. Min Mag (Lond) 61:271–283

Carosi R, Gattiglio M, Musumeci G, Oggiano G (1992) Geologia della catena ercinica in Sardegna—Zona a falde. Guida all'escursione: "Struttura della Catena Ercinica in Sardegna", 24–29 Maggio 1992, 77–108

Carten RB (1986) Sodium–calcium metasomatism: chemical, temporal, and spatial relationships at the Yerington, Nevada porphyry copper deposit. Econ Geol 81:1495–1519

Castorina F, and Petrini R (1989) Radiometric geochronology: some constraints to the isochron method by the iterative least-squares approach. Geochem J 23:101–109

Cathelineau M (1987) U–Th-REE mobility during albitization and quartz dissolution in granitoids: evidence from southeast French Massif Central. Bull Min 110:249–259

Cathelineau M (1988) Accessory mineral alteration in peraluminous granites at the hydrothermal stage: a review. Rend Soc Ital Mineral Petrol 43:499–508

Charoy B, Pollard PJ (1989) Albite-rich, silica-depleted metasomatic rocks at Emuford, northeast Queensland: mineralogical, geochemical and fluid inclusion constraints on hydrothermal evolution and tin mineralization. Econ Geol 84:1850–1874

Chauris L (1985) Premières données géochimiques sur les albitites metasomatiques des environs de Brest (Finistère, France). Bull Soc Géol Fr 8:885–889

Cheilletz A, Giuliani G (1982) Rôle de la déformation du granite dans la genèse des episyénites feldspathiques des massifs de Lovios-Geres (Galice) et des Zaer (Maroc Central). Miner Depos 17:387–400

Del Moro A, Di Simplicio P, Ghezzo C, Guasparri G, Rita F, Sabatini G (1975) Radiometric data and intrusive sequence in Sardinian Batholith. Neues Jahrb Mineral Abh 126:28–44

Dilles JH, Einaudi MT (1992) Wall-rock alteration and hydrothermal flow paths about the Ann-Mason porphyry copper deposit, Nevada—a 6-km vertical reconstruction. Econ Geol 87:1963–2001

Dilles JH, Farmer GL, Field CW (1995) Sodium–calcium alteration due to no-magmatic saline fluids in porphyry copper deposits: results from Yerington, Nevada. In: Thompson JFP (ed) Magmas, fluids, and ore deposits. Miner Ass Canada Short Course 23:309–338

Elter FM, Franceschelli M, Ghezzo C, Memmi I, Ricci CA (1986) The geology of Northern Sardinia. Final Meeting of IGCP, May 26–31, 1986, Newsletter:87–97 (special issue)

Fadda R (1994) The epithermal system of the south-western Montiferru area (central western Sardinia): wallrock alteration and metallic mineralization. Plinius (Milano) 11:132–137

Fadda S, Rivoldini S, Cau I (1995) ICP-MS determination of 45 trace elements in whole coal using microwave oven acid digestion for sample preparation. Geostand Newsl XIX (1):41–54

Grant JA (1986) The isocon diagram—a simple solution to Greisens' equation for metasomatic alteration. Econ Geol 81:1976–1982

Green TH, Pearson NJ (1986) Rare earth elements partitioning between sphene and coexisting silicate liquid at high pressure and temperature. Chem Geol 55:105–119

Johnson JP, Mc Culloch MT (1995) Sources of mineralising fluids for the Olympic Dam deposit (South Australia): Sm–Nd isotopic constraints. Chem Geol 121:177–199

Kovalenko VI (1978) The genesis of rare metal granitoids and related ore deposits. In: Stemprok M, Burnol L, Tischendorf G (eds) Metallization associated with acid magmatism. Czech Geol Surv 3:235–247

Leroy J, Turpin L (1988) REE, Th and U behaviour during hydrothermal and supergene processes in a granite environment. Chem Geol 68:239–251

Leitch CHB, Lentz DR (1994) The Greisens approach to mass balance constraints of alteration systems: methods, pitfalls, examples. In: Lentz D (ed) Alteration and alteration processes associated with ore-forming systems. Geol Ass Can 11:161–192 (Short course)

Ludwig KR (1995) Isoplot: a plotting and regression program for radiogenic isotope data. Version 2.82. US Geol Surv (open file, report) 91–445

Maccioni L, Marchi M, Padalino G, Palomba M, Sistu G (1995) Bentonite occurrences in the Tertiary volcanic rocks in central Sardinia, Italy. Explor Min Geol 4(1):74–79

Montoya JW, Hemley JJ (1975) Activity relations and stabilities in alkali feldspar and mica alteration reactions. Econ Geol 70:577–594

Morad S, Bergan M, Knarud R, Nystuen JP (1990) Albitization of detrital plagioclase in Triassic reservoir sandstones from the Snorre Field, Norwegian North Sea. J Sediment Petrol 60:411–425

Orville PM (1963) Alkali ion exchange between vapor and feldspar phases. Am J Sci 261:201–237

Orville PM (1972) Plagioclase cation exchange equilibria with aqueous chloride solution: results at 700°C and 2000 bars in the presence of quartz. Am J Sci 272:234–272

Padalino G, Palomba M (1999) La distribuzione delle terre rare nelle albititi dell'area di Sarule-Ottana (Sardegna centrale, Italia). Mineral Petrogr Acta XLII:1–15

Palomba M (2001). Geological, mineralogical, geochemical features and genesis of the albitite deposits of central Sardinia (Italy). In: Frau F (ed) Guidebook to the field trips in Sardinia of the WRI 10, Rend Semin Fac Sci R Univ Cagliari LXXI (2):35–57 (Special issue)

Pan Y, Fleet ME (1991) Vanadian allanite-(La) and vanadian allanite-(Ce) from the Hemlo gold deposit, Ontario, Canada. Min Mag 55:497–507

Petersson J, Eliasson TH (1997) Mineral evolution and element mobility during episyenitization (dequartzification) and albitization in the postkinematic Bohus granite, southwest Sweden. Lithos 42:123–146

Potter MJ (2004) Mineral commodity summaries. US Geol Surv, January 2004, 60–61

Schade J, Cornell DH, Theart HFJ (1989) Rare earth elements and isotopic evidence for the genesis of the Prieska massive sulfide deposit, South Africa. Econ Geol 84:49–63

Schoch AE, Scheepers R (1990) The distribution of uranium and thorium in the Cape Columbine granite from the southwestern Cape Province, South Africa. Ore Geol Rev 5:223–246

Schwartz MO (1992) Geochemical criteria for distinguishing magmatic and metasomatic albite-enrichment in granitoids: examples from the Ta–Li granite Yichun (China) and the Sn–W deposit Tikus (Indonesia). Miner Depos 27:101–108

Simeone R, Simmons SF (1999) Mineralogical and fluid inclusion studies of low-sulphidation epithermal veins at Osilo (Sardinia, Italy). Miner Depos 34:705–717

Simeone R, Dilles J, Padalino G, Palomba M (2003) Mineralogical and stable isotope studies of kaolin deposits: shallow epithermal systems of western Sardinia (Italy). Econ Geol 100:115–130

Slaby E (1992) Changes in the structural state of secondary albite during progressive albitization. Neues Jahrb Mineral Monatsh 321–335

Sun SS, Mc Donough WF (1989) Chemical and isotopic systematics of oceanic basalts: implications for mantle composition and processes. In: Saunders AD, Norry MJ (eds) Magmatism in the ocean basins. J Geol Soc (Lond) 42:313–345 (Special publication)

Taylor RP, Fryer BJ (1983) Rare earth elements lithogeochemistry of granitoid mineral deposits. Can Min Metall Bull 76:74–84

Tommasini S, Poli G, Halliday AN (1995) The role of sediment subduction and crustal growth in Hercynian plutonism: isotopic and trace element evidence from the Sardinia–Corsica batholith. J Petrol 36(5):1305–1332

Tulloch AJ (1979) Secondary Ca–Al silicates as low-grade alteration products of granitoid biotite. Contrib Mineral Petrol 69:105–117

Turpin L, Maruejol P, Cuney M (1988) U–Pb, Rb–Sr and Sm–Nd chronology of granitic basement, hydrothermal albitites and uranium mineralization (Lagoa Real, South Bahia, Brazil). Contrib Mineral Petrol 98:139–147

Turpin L, Leroy JL, Sheppard SMF (1991) Isotopic systematics (O, H, C, Sr, Nd) of superimposed barren and U-bearing hydrothermal systems in a Hercynian granite, Massif Central, France. Chem Geol 88:85–98

White WM, Patchett PJ (1984) Hf–Nd–Sr isotopes and incompatible element abundances in island arcs: implications for magma origins and crust-mantle evolution. Earth Planet Sci Lett 67:167–185

Wood SA (1990a) The aqueous geochemistry of the rare-earth elements and yttrium I. Chem Geol 82:159–186

Wood SA (1990b) The aqueous geochemistry of the rare-earth elements and yttrium II. Chem Geol 88:99–125